Power Amplifiers' Model Assessment and Memory Effects Intensity Quantification Using Memoryless Post-Compensation Technique

Oualid Hammi, *Student Member, IEEE*, Scott Carichner, *Member, IEEE*, Bill Vassilakis, *Senior Member, IEEE*, and Fadhel M. Ghannouchi, *Fellow, IEEE*

***Abstract*—A novel approach for power amplifiers static nonlinearity characterization in the presence of memory effects is presented. A subsampling technique is used to reduce the bandwidth of the test signal without changing the waveform characteristics. This cancels the memory effects of the amplifier without affecting its static behavior. Memoryless AM/AM and AM/PM characteristics are measured as a function of the carrier frequency. This points out the contribution of the frequency dependency of the amplifier's static nonlinearity to its behavior under wideband signal drive. A memoryless post-compensation technique is then introduced to accurately assess the performance of several behavioral models. In fact, it is demonstrated that direct comparison of the measured output of the device-under-test with the estimated output does not provide reliable assessment of the model performance. Conversely, memoryless post-compensation efficiently differentiates the performance of these models. To provide a comprehensive approach for model validation and prototype performance evaluation, memory effects intensity metrics are introduced. These metrics are applied to evaluate the memory effects present in a 300-W peak power Doherty amplifier driven by various multicarrier wideband code division multiple access signals.**

***Index Terms*—Behavioral modeling, digital predistortion, linearization, memory effects, post-compensation, power amplifier (PA), static nonlinearity, third generation (3G), wideband code division multiple access (WCDMA).**

I. Introduction

BEHAVIORAL modeling of RF power amplifiers (PAs) is an essential task in the design of high-performance wireless transmitters that combine high power efficiency and spectrum compliant linearity performance. This is even more important in modern communication systems that employ envelope-varying signals with high peak-to-average power ratios (PAPRs). In fact, such signals set stringent linearity requirements on the PA and usually lead to the sacrifice of the system's power efficiency in order to meet the linearity requirements. In this context, behavioral modeling of the PA/transmitter is a time and resource efficient post-prototyping process that is primarily used for the transmitters' performance estimation and the design of the linearizer.

In base-station transmitters, the wide bandwidth necessary for multicarrier and full-band PAs makes the memory effects unavoidable in the observed PA behavior. Numerous behavioral models that take into account memory effects have been proposed in the open literature. These include memory polynomials, Volterra series, Wiener and Hammerstein models, and multidimensional lookup table (LUT)-based models [1]–[5]. Even though model validation is a crucial step, the standard procedure that is being used consists of comparing the estimated signal at the output of the model to the measured signal at the output of the device-under-test (DUT). However, the direct comparison of the measured and estimated output signals usually shows a minor difference between the performance of the different models, even when memoryless models are compared to models that take into account memory effects. Indeed, the contribution of the memory effects to the PA's output is usually significantly lower than that of the static nonlinearity. Accordingly, the direct comparison method is not a reliable approach for model assessment in PAs exhibiting memory effects. In [8], a model assessment method in which memoryless digital predistortion is applied to the input signal used to drive the model and DUT was proposed. The use of the memoryless predistorter cancels the contribution of the static nonlinearity to the signals at the output of both the model and DUT. Thus, the remaining nonlinearity is that due to the memory effects. Comparing the residual nonlinearities was shown to be an accurate method for model performance assessment.

In addition, it is also important to quantify memory effects in RF PAs/transmitters. This is useful for the estimation of the linearity performance that can be achieved through memoryless digital predistortion. Moreover, memory effects intensity (MEI) measurement can be used as a metric to compare the linearizability of different PA prototypes and the memory effects characteristics of different technologies, such as LDMOS and GaN [6]. Several approaches have been proposed for memory effects quantification [6]–[16]. Most of these are defined under a multitone input signal and are mainly based on the observed spectral asymmetry. In [8], memoryless digital predistortion has been

Manuscript received April 25, 2008; revised July 02, 2008. First published November 07, 2008; current version published December 05, 2008. This work was supported by the Alberta Informatics Circle of Research Excellence (iCORE), the Natural Sciences and Engineering Research Council of Canada (NSERC), the Canada Research Chair (CRC) Program, and TRLabs.

O. Hammi and F. M. Ghannouchi are with the iRadio Laboratory, Department of Electrical and Computer Engineering, Schulich School of Engineering, University of Calgary, Calgary, AB, Canada T2N 1N4 (e-mail: ohammi@ucalgary.ca; fadhel.ghannouchi@ucalgary.ca).

S. Carichner and B. Vassilakis are with Powerwave Technologies Inc., Santa Ana, CA 92705 USA (e-mail: Scott.Carichner@pwav.com; Bill.Vassilakis@pwav.com).

Color versions of one or more of the figures in this paper are available online at http://ieeexplore.ieee.org.

Digital Object Identifier 10.1109/TMTT.2008.2006809

applied for the quantification of MEI under a modulated input signal. Consequently, memoryless digital predistortion is currently the standard technique used in PAs/transmitters model accuracy assessment and MEI quantification. However, this technique has a major disadvantage: it requires more than one set of measurements. A first set of measurements is needed to characterize the DUT and derive both the forward model and the memoryless digital predistorter (DPD). A second set of measurements is then needed to capture the signal at the output of the DUT when memoryless digital predistortion is applied. Furthermore, in practice, more than two sets of measurements are needed since the synthesis of the memoryless digital predistortion function, both in open- and closed-loop DPD configurations, requires more than one iteration.

In this study, a memoryless post-compensation technique is introduced for model assessment and MEI quantification. The major advantage of the proposed approach is that it only requires a single set of measurements. In fact, following the characterization of the DUT, the forward model and the memoryless post-compensator are derived. For model validation and MEI measurements, the post-compensator is applied to the estimated signal at the output of the model and to the measured signal at the output of the DUT. Accordingly, model validation and MEI measurements are performed within simulation software and do not call for additional measurements. The post-compensation technique, as well as the memoryless digital predistortion technique, uses the static nonlinearity of the DUT to generate the post-compensation function. Thus, it is clear that the precision and performance of this technique depend on the accuracy in the extraction of the static behavior of the DUT. In [17], the authors presented a novel approach for the accurate extraction of the static nonlinearity when memory effects are present. This technique is applied in this study for the synthesis of the post-compensation function.

In this paper, the static nonlinearity extraction technique is applied for the accurate characterization of the memoryless behavior of the DUT. It is also used to characterize the frequency dependency of the memoryless behavior of the DUT. The post-compensation technique is then introduced and applied in the performance evaluation of various behavioral models of an experimental Doherty amplifier. The MEI of this amplifier is then estimated under several multicarrier drive signals using the post-compensation technique. In Section II, the DUT and the measurement system are introduced. The accurate static nonlinearity extraction technique is presented in Section III and is used to characterize the static DUT behavior over a 60-MHz frequency band. In Section IV, the post-compensation technique is introduced and applied in model accuracy assessment. The MEI of the DUT is evaluated in Section V, and conclusions are presented in Section VI.

II. Measurement Setup and Tools

The measurement setup used in this study is presented in Fig. 1. It is based on the instantaneous complex input and output waveforms measurement technique proposed in [18]. The experimental setup is composed of the DUT, a vector signal generator, a vector signal analyzer (VSA) and a computer that monitors the measurements through Nonlinear

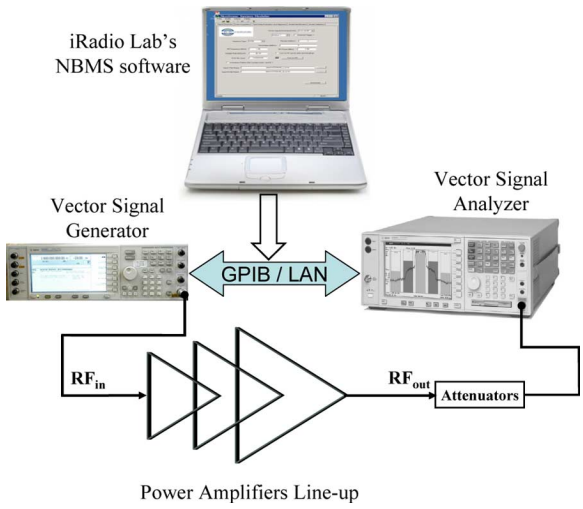

Fig. 1. Measurement setup.

Behavioral Modeling Software (NBMS), which was developed by the iRadio Laboratory, University of Calgary, Calgary, AB, Canada. This software is used to download the signal waveform into the vector signal generator that feeds the DUT with the corresponding RF signal. The measured signal at the output of the DUT is acquired by NBMS from the VSA software. The time delay between the input and output waveforms is estimated and compensated for according to the method described in [9]. The extraction of the different models considered in this study (memoryless LUT, memory polynomials, Hammerstein, Wiener, augmented Hammerstein and augmented Wiener models) is performed using this software. The memoryless post-compensation technique was developed and implemented in this software for model validation.

The DUT is a high-power high-efficiency LDMOS-based Doherty amplifier with 300-W peak power and 61-dB small-signal gain. This PA is designed for operation in the 2110–2170-MHz frequency band. During the tests, several WCDMA signals generated using Test Model 1, having 1–4 carriers, were applied to the DUT. The configurations of the WCDMA signals used are 010 for the one-carrier signal, 0110 for the two-carrier signal, 101 and 111 for the three-carrier signals, and 1111 and 1001 for the four-carrier signals (where 1 denotes an ON carrier and 0 denotes an OFF carrier). All these waveforms are 2-ms long and are sampled at 92.16 MHz.

III. Accurate Extraction of PA's Static Nonlinearity

The identification of the memoryless nonlinearity in RF PAs exhibiting memory effects is necessary for two-box modeling (Hammerstein- and Wiener-based models), as well as the quantification of the memory effects contribution to the overall nonlinearity exhibited by the PA. In [17], the authors introduced a novel approach for static nonlinearity extraction. This consisted of cancelling the memory effects without changing the static behavior of the PA. In fact, the nonlinear behavior of a PA is a function of the operating carrier frequency and the input signal's characteristics (mainly its average power, statistics, and bandwidth). For a given carrier frequency, the bandwidth of the signal only affects the memory effects exhibited by the PA, but not its

static nonlinearity. Accordingly, it is possible to measure the static nonlinearity of the PA if the bandwidth of the input signal is reduced enough to minimize the electrical memory effects exhibited by the PA, while keeping the waveform average power and statistics unchanged. The choice of the signal's bandwidth to be applied for the static nonlinearity measurement should also take into account the thermal memory effects that arise when narrowband signals are used. Thus, the bandwidth of the drive signal should be narrow enough to minimize electrical memory effects, but wide enough to avoid thermal memory effects. Typically, the test signal should have a bandwidth in the range of 1 MHz in order to simultaneously minimize both the electrical and thermal memory effects. In fact, electrical memory effects appear as the bandwidth of the signal increases, while thermal memory effects are observed for narrowband signals. Thermal memory effects have several frequency ranges and their time constants are typically in the order of 1 ms and 10 μs. These are completely determined by the mechanical configuration of the transistor die structure and mounting to its package. Physically, the upper limit of the thermal memory effects frequency range is around few 100 kHz. Electrical memory effects usually appear for bandwidths of more than 1 MHz. This offers a sweet spot for the bandwidth of the test signal for which both the electrical and thermal memory effects will be significantly low. In addition, a careful design would minimize these effects (push the thermal memory effects toward narrower bandwidths and electrical memory effects toward wider bandwidths) and avoid that they overlap in frequency. Thermal memory effects can be minimized by appropriate thermal grounding and mechanical design, and electrical memory effects can be minimized by a careful design of the bias and matching networks. These two aspects were considered in the design of the PA prototype used in this study.

The sampling rate of the baseband waveform can be changed in order to independently control the input signal's bandwidth without affecting its average power and statistics. Indeed, the signal's average power and its statistics are fully defined by the waveform data samples and not the sampling rate. To extract the static nonlinearity of the DUT, a one-carrier wideband code division multiple access (WCDMA) signal with a 3.84-MHz bandwidth was used. The sampling rate scaling factor (α), defined as the ratio between the actual sampling frequency (f_s') and the original sampling frequency (f_s), was varied. Equivalently, α is also the ratio between the actual bandwidth (BW') of the signal and its original bandwidth (BW)

$$\alpha = \frac{f_s'}{f_s} = \frac{\mathrm{BW}'}{\mathrm{BW}}. \tag{1}$$

Fig. 2 presents the measured AM/AM and AM/PM curves of the DUT for different values of the sampling rate scaling factor ($\alpha = 1.0, 0.6$, and 0.2). The AM/AM and AM/PM curves were obtained for the raw measured data using the same moving average fitting algorithm [9]. According to this data, the averaged AM/AM characteristics are significantly biased by the memory effects, but the AM/PM characteristics are not.

The "true" static nonlinearity of the DUT is the one measured for $\alpha = 0.2$ since it was found that the DUT does not exhibit any memory effects when driven by the corresponding test signal

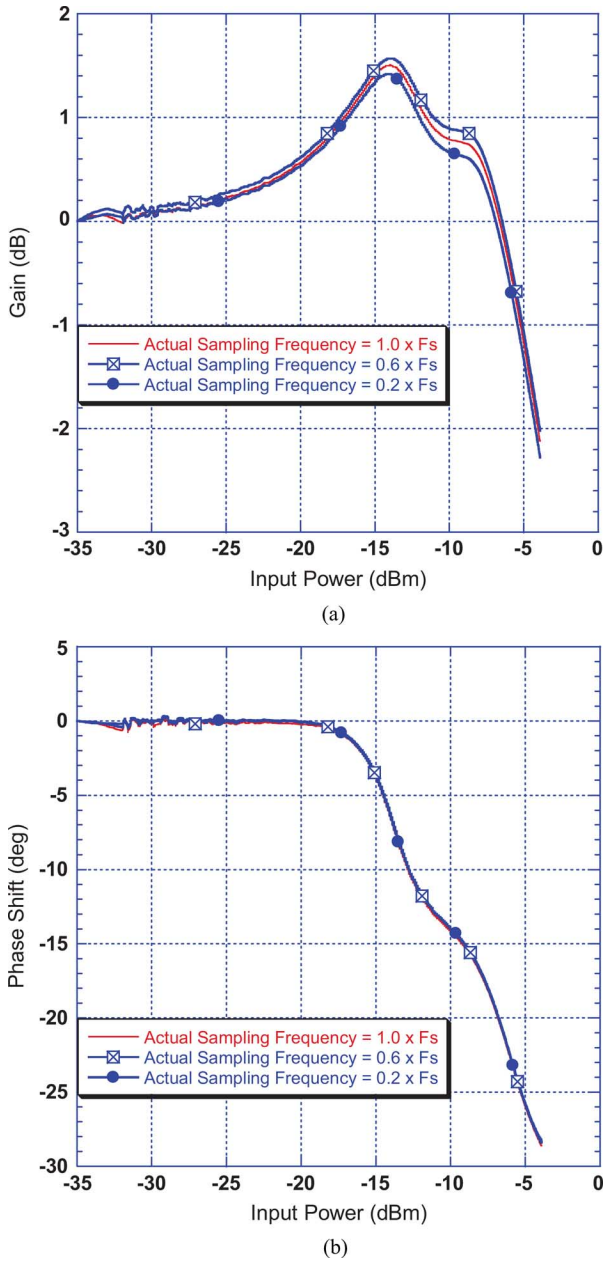

Fig. 2. PA's measured characteristics versus signal bandwidth. (a) AM/AM characteristics. (b) AM/PM characteristics.

[17]. The raw measured AM/AM and AM/PM data can be used to detect the presence of memory effects. Indeed, the hysteresis phenomenon due to the variation of the instantaneous gain as a function of the previous samples appears as a dispersion in the AM/AM and AM/PM curves. Fig. 3(a) presents the raw measured AM/AM curves of the DUT for the cases of $\alpha = 1.0$ and $\alpha = 0.2$. The measured data for $\alpha = 1.0$ overlays on that corresponding to $\alpha = 0.2$ and presents slightly higher dispersion. In fact, for $\alpha = 1.0$, memory effects exist, but are relatively weak, and thus, not easy to detect by observing the dispersion on the AM/AM curves. A more accurate way to detect the memory effects and assess the memory-effects-free behavior of the PA consists in using memoryless predistortion, as presented in [17], or equivalently memoryless post-compensation, as described in

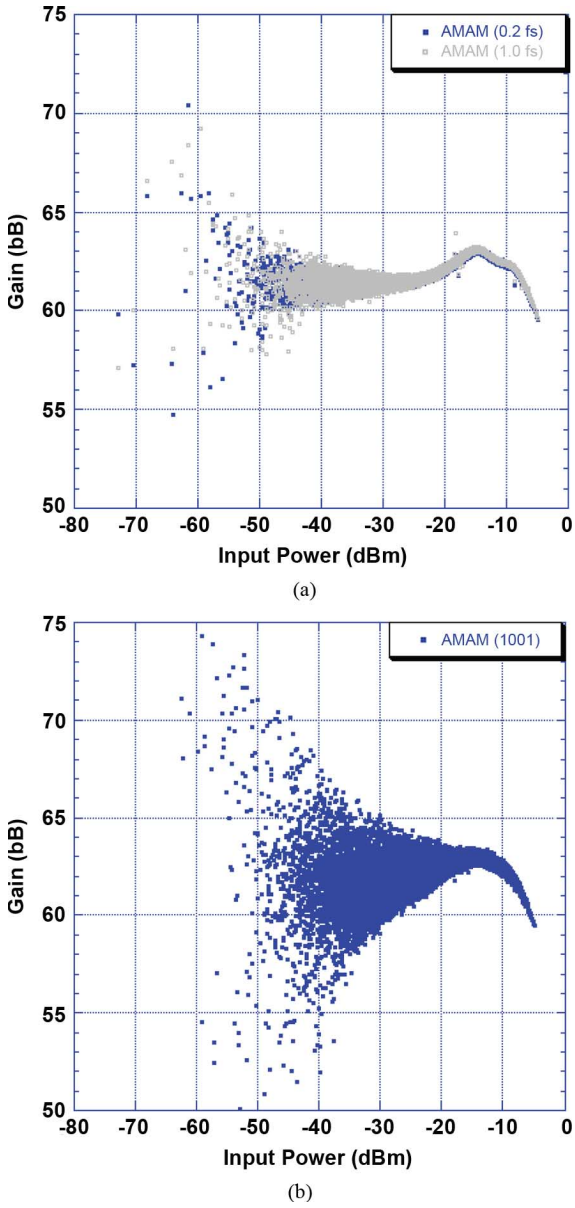

Fig. 3. Raw measured AM/AM characteristics versus signal bandwidth. (a) $\alpha = 1.0$ and $\alpha = 0.2$. (b) Four-carrier WCDMA.

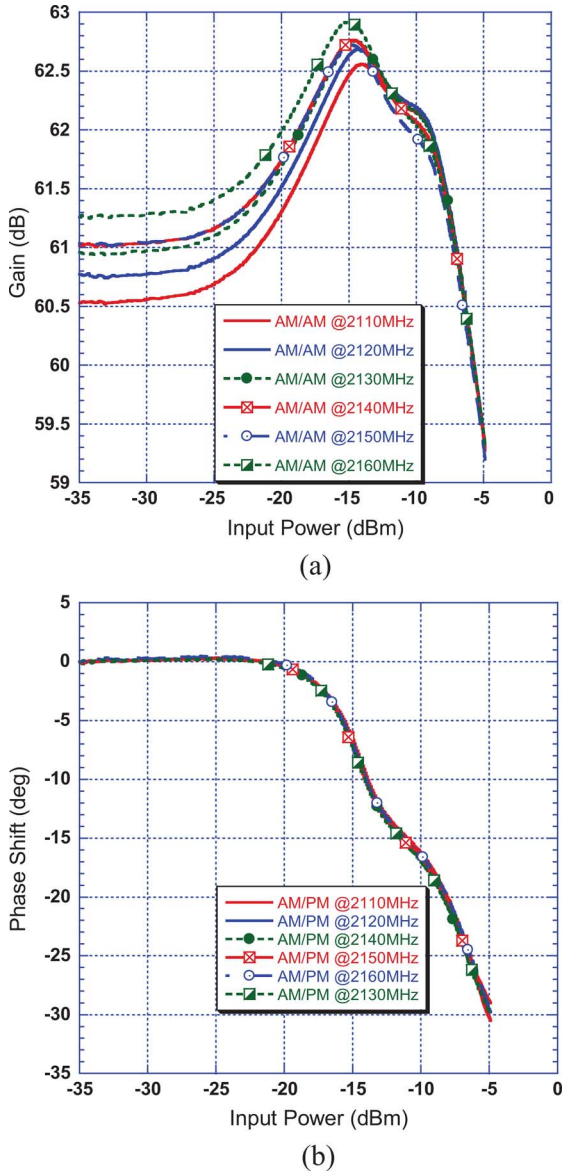

Fig. 4. PA's measured characteristics versus carrier frequency. (a) AM/AM characteristics. (b) AM/PM characteristics.

Section IV. In Fig. 3(b), the raw measured AM/AM curve obtained under a four-carrier WCDMA excitation signal is shown. This figure clearly illustrates the dispersion caused by memory effects as they become significant due to the wide bandwidth of the test signal.

To extend the study of the static behavior of the PA and its memory effects, further measurements were performed. These consisted of measuring the static AM/AM and AM/PM of the DUT, using the accurate subsampling-based static nonlinearity extraction technique, over the entire 60-MHz bandwidth of the 2100-MHz frequency band. For this purpose, the memoryless AM/AM and AM/PM characteristics of the DUT were extracted, as a function of the carrier frequency, from 2110 to 2170 MHz, in steps of 5 MHz. Fig. 4 reports the measured results. For clarity reasons, only part of the measured curves is plotted. According to this figure, there is a significant frequency dependency of the AM/AM characteristics of the PA. Moreover, this shows that the small-signal gain of the DUT, as well as its nonlinearity shape, depend on the carrier frequency. To investigate the impact of this frequency dependency on the linearizability of the DUT, the normalized static AM/AM characteristics were plotted as a function of the carrier frequency in Fig. 5. This figure clearly illustrates that, in addition to the small-signal gain variation, the static nonlinearity of the amplifier also varies as a function of the carrier frequency. A linear equalizer can be used to address the flatness problem of the small-signal gain, but not the frequency dependency of the nonlinear shape. The nonlinearity shape variation as a function of the carrier frequency adds up or might be part of the commonly known memory effects when wideband input signals are used. This phenomenon has to be dealt with for accurate wideband modeling and linearization purposes. Further investigations are needed to determine whether it contributes or not to the memory effects exhibited by the PA as commonly defined (dependency of the current output sample on the preceding samples).

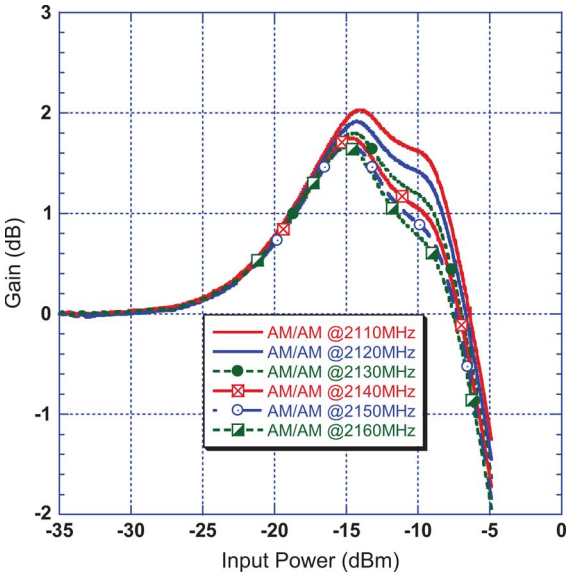

Fig. 5. Normalized AM/AM characteristics versus carrier frequency.

A memoryless DPD, synthesized using the measured AM/AM and AM/PM characteristics at 2140 MHz (center of the 2100-MHz band), was then used to estimate the performance of the linearized amplifier as the carrier frequency of the drive signal was varied. As expected from the frequency-dependant AM/AM characteristics, significant residual nonlinearity is obtained as the carrier frequency is shifted away from the center frequency used to synthesize the memoryless predistorter. According to Fig. 6(a), approximately 20-dBc adjacent channel power ratio (ACPR) degradation is observed for a 30-MHz frequency offset. Furthermore, if a 20-MHz bandwidth (case of a four-carrier WCDMA signal) is considered [see Fig. 6(b)], the ACPR performance is decreased by up to 10 dBc.

IV. Post-Compensation Technique for Model Accuracy Assessment

The contribution of the memoryless nonlinearity dominates the overall nonlinearity observed at the output of PAs exhibiting memory effects. Accordingly, it is not possible to accurately evaluate PA memory effects modeling in the presence of memoryless nonlinearities. Thus, it is necessary to compensate for the memoryless behavior of the PA prior to the model validation step. Static nonlinearity cancellation by means of memoryless digital predistortion was proven to be an accurate technique for PA model performance assessment [7]–[10]. However, the main disadvantage of this technique is that it requires first the synthesis of the predistortion function and then the measurement of the PA output signal when memoryless predistortion is applied. In order to overcome this iterative measurement process, memoryless post-compensation is proposed to cancel the static nonlinearity at the output of the amplifier rather than its input. Even though such a technique cannot be implemented in practice for PA linearization due to the high power levels involved at the output of PAs, its use within a simulation environment for model assessment alleviates the need for extra measurements. Indeed, as shown in Fig. 7, which illustrates the principle of

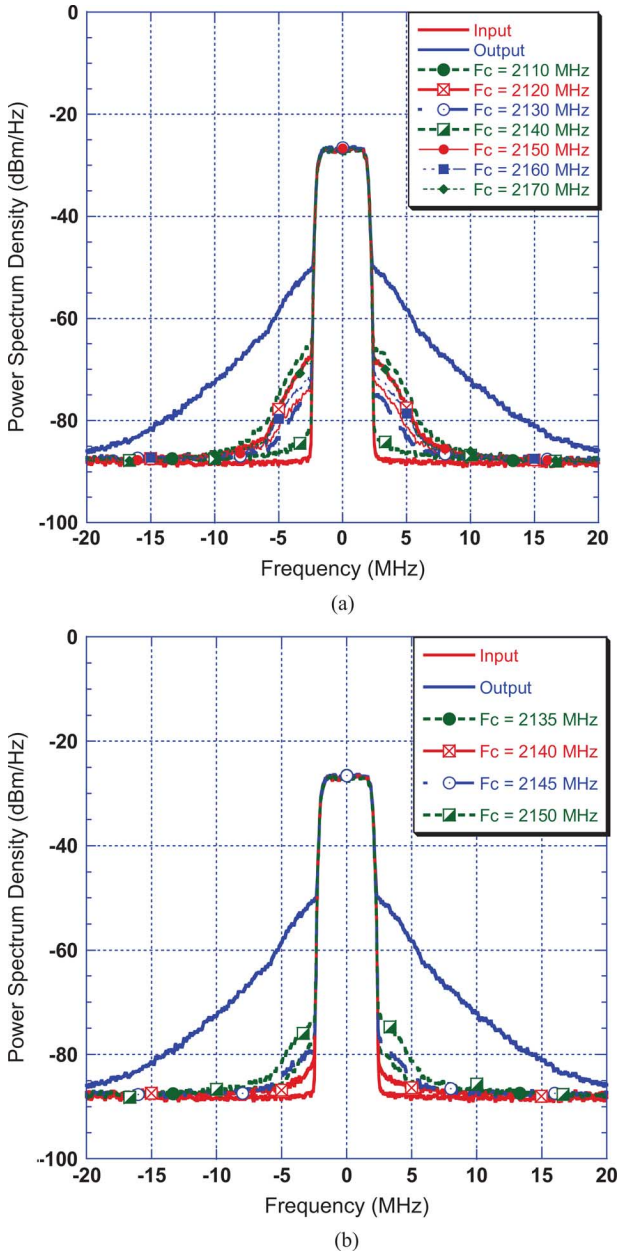

Fig. 6. Spectra at the output of the DUT after memoryless predistortion versus carrier frequency. (a) Over 60-MHz bandwidth. (b) Over 20-MHz bandwidth.

the post-compensation technique for model validation, the PA is first characterized under the test signal. The input and output data files captured during this single measurement process are then processed to extract the DUT models, as well as the memoryless post-compensator. The measured signal at the output of the PA and the estimated signals at the output of each model are then fed successively to the memoryless post-compensator to calculate the corresponding post-compensated signals. The synthesis of the memoryless post-compensation function from the measured DUT input and output data is similar to that of the memoryless DPD. The main difference is that the DPD's output power is aligned with the PA's input power, while the post-compensator's input power is aligned with the PA's output power.

The measurements performed under a four-carrier WCDMA input signal were used to synthesize six models of the DUT.

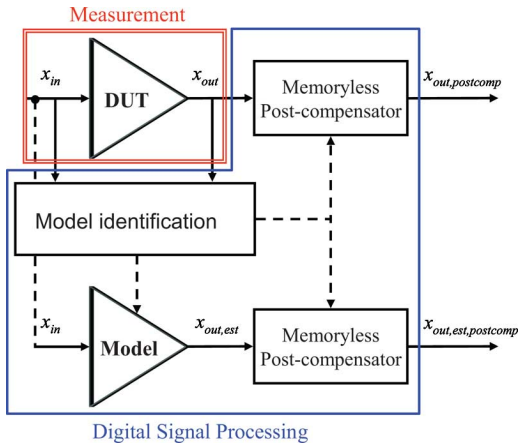

Fig. 7. Block diagram of the memoryless post-compensation technique.

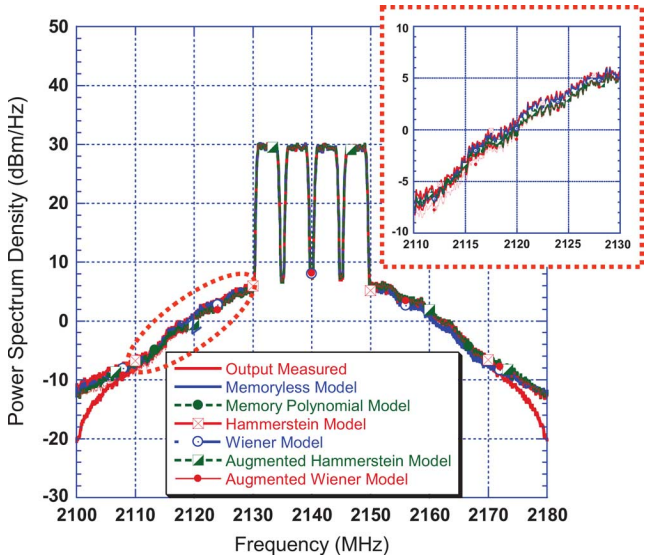

Fig. 8. Measured and estimated output spectra before post-compensation.

These models are the memoryless LUT, the memory polynomials model (three branches, twelfth-order nonlinearity in each branch), the Wiener model (three-tap finite-impulse response (FIR) filter followed by the memoryless model), the Hammerstein model (memoryless model followed by a three-tap FIR filter), the augmented Wiener model (two FIR filters with three taps each, followed by the memoryless model), and the augmented Hammerstein model (memoryless model followed by two FIR filters with three taps each). The estimated output spectra obtained using these models are plotted in Fig. 8. This figure also shows the measured spectra at the output of the DUT. According to this figure, all models seem to have similar performance. The errors between the measured data and the different models outside the 60-MHz frequency band centered on the carrier frequency are mainly attributed to the limited bandwidth of the receiver used during the characterization step.

To efficiently compare the performance of the considered models, memoryless post-compensation was applied to the estimated and measured PA output signals. The spectra of the corresponding post-compensated signals are presented in Fig. 9, which demonstrates the effectiveness of the proposed

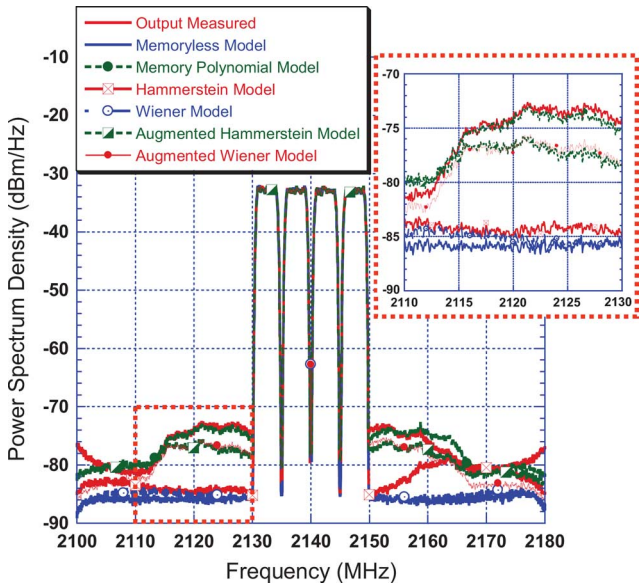

Fig. 9. Measured and estimated output spectra after post-compensation.

memoryless post-compensation technique to differentiate the performance of the various models. In fact, the memory polynomial model is found to be the most accurate in predicting the PA behavior. The ability of augmented Hammerstein and augmented Wiener models to model the memory effects exhibited by the DUT is slightly worse. Moreover, when post-compensation is applied to the signal at the output of the memoryless model, there is no residual nonlinearity at the output of the post-compensator. This is expected since the post-compensator was designed to fully cancel the memoryless behavior of the PA. Accordingly, even though the direct comparison of the PA's measured output and the models' estimated outputs did not show the limitation of some models, the memoryless post-compensation makes it possible to accurately assess the performance of these models and their ability to predict the memory effects exhibited by the DUT.

Time-domain metrics such as the normalized mean square error (NMSE) can also be applied to assess the accuracy of the considered models and compare their performances. Table I reports the calculated NMSE for the various models before and after post-compensation. These results show that the use of the NMSE does not clearly illustrate the relative performance of the models. Indeed, in the time domain, both the useful signal resulting from the linear amplification of the input signal and the error signal are overlaid. However, in the frequency domain, nonlinear distortions and the useful signal correspond to two different frequency ranges. Thus, frequency-domain data are more appropriate for model performance assessment and comparison.

V. MEI Quantification

When driven by the measured signal at the output of the DUT, the memoryless post-compensator cancels the DUT's static nonlinearity. Accordingly, the residual nonlinearity present in the signal at the output of the post-compensator is solely due to memory effects. In fact, as shown in Fig. 9, the PA's input signal is fully recovered after applying post-compensation to

TABLE I
NMSE VERSUS DUT MODEL

	Before Post-compensation (dB)	After Post-compensation (dB)
Model ⇩		
Memoryless	-40.37	-42.90
Memory Polynomial	-45.62	-47.51
Hammerstein	-43.56	-44.97
Wiener	-43.79	-45.15
Augmented Hammerstein	-45.09	-46.96
Augmented Wiener	-45.27	-47.18

the DUT memoryless model's output signal. Thus, it is possible to quantify the memory effects present at the output of the PA by applying the proposed memoryless post-compensation technique. The DUT input and output measured waveforms, as well as the signal obtained at the output of the post-compensator, are plotted in Fig. 10 for a single-carrier and a four-carrier (1001 configuration) WCDMA signals. This figure shows the residual nonlinearity due to memory effects present in the signal at the output of the DUT. The MEI is very low for the single-carrier signal, but is significant in the case of the multicarrier signal. The accurate quantification of these memory effects is crucial for the objective comparison of different PA prototypes designed using different architectures or different technologies. This also provides a valuable indication of the performance that can be achieved by using memoryless DPDs.

The proposed MEI metric is based on power integration in the channel (in-band), the adjacent channel (mainly attributed to third-order intermodulation), and the alternate adjacent channel (mainly attributed to fifth-order intermodulation), as illustrated in Fig. 11.

For a multicarrier signal, the MEI within the adjacent channel and the alternate adjacent channel frequency bands are defined by (2) and (3), shown at the bottom of this page, where: 1) $\mathrm{MEI}_{\mathrm{AdjCha}}$ is the MEI in the adjacent channel; 2) $\mathrm{MEI}_{\mathrm{AltAdjCha}}$ is the MEI in the alternate adjacent channel; 3) $P(f)$ is the power spectrum density of the considered signal; 4) M is the number of active carriers; 5) f_{ci} and BW_i are the center frequency and the bandwidth of the active carriers, respectively; 6) $f_{c\,\min}$ and $f_{c\,\max}$ are the lowest and highest center frequencies of the active carriers, respectively;

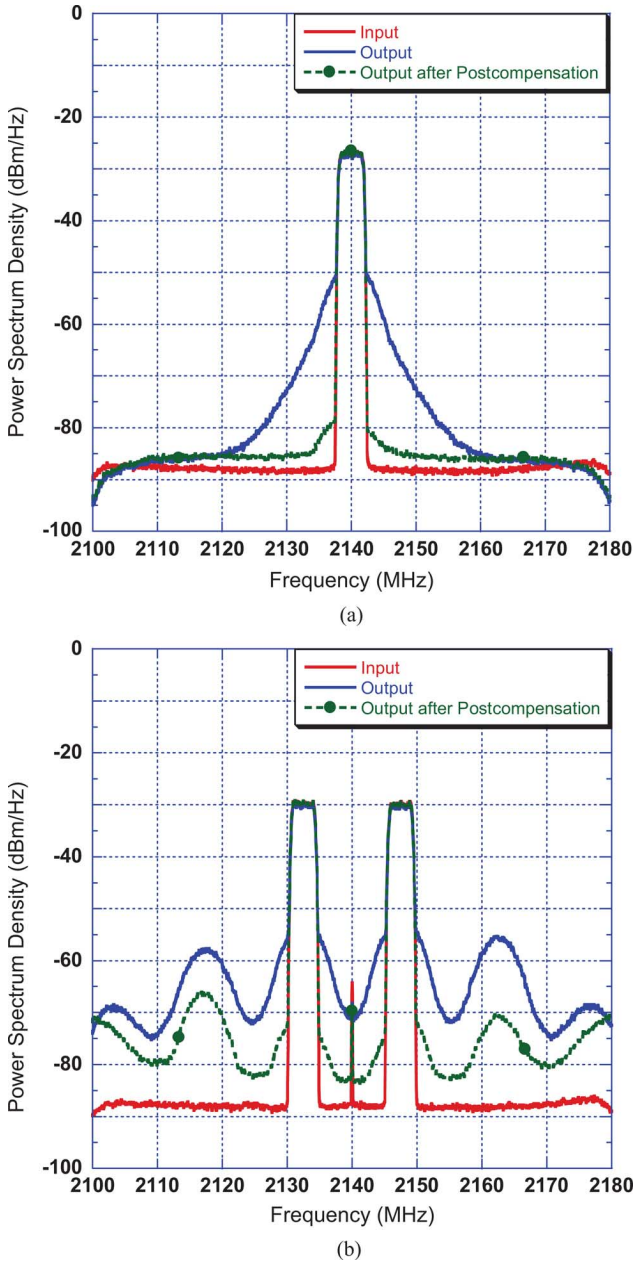

Fig. 10. Residual nonlinearity after memoryless post-compensation. (a) One-carrier WCDMA signal. (b) Four-carrier (1001) WCDMA signal.

$$\mathrm{MEI}_{\mathrm{AdjCha}} = \left[\sum_{i=1}^{M}\int_{f_{ci}-\mathrm{BW}_i/2}^{f_{ci}+\mathrm{BW}_i/2} P(f)\cdot df\right]_{\mathrm{dBW}} - \left[\begin{array}{l}\int_{f_{c\,\min}-(\mathrm{BW}_{f_{c\,\min}}/2)-\mathrm{BW}_{\mathrm{Tot}}}^{f_{c\,\min}-\mathrm{BW}_{f_{c\,\min}}/2} P(f)\cdot df \\ +\int_{f_{c\,\max}+\mathrm{BW}_{f_{c\,\max}}/2}^{f_{c\,\max}+(\mathrm{BW}_{f_{c\,\max}}/2)+\mathrm{BW}_{\mathrm{Tot}}} P(f)\cdot df\end{array}\right]_{\mathrm{dBW}} \tag{2}$$

$$\mathrm{MEI}_{\mathrm{AltAdjCha}} = \left[\sum_{i=1}^{M}\int_{f_{ci}-\mathrm{BW}_i/2}^{f_{ci}+\mathrm{BW}_i/2} P(f)\cdot df\right]_{\mathrm{dBW}} - \left[\begin{array}{l}\int_{f_{c\,\min}-(\mathrm{BW}_{f_{c\,\min}}/2)-2\mathrm{BW}_{\mathrm{Tot}}}^{f_{c\,\min}-(\mathrm{BW}_{f_{c\,\min}}/2)-\mathrm{BW}_{\mathrm{Tot}}} P(f)\cdot df \\ +\int_{f_{c\,\max}+(\mathrm{BW}_{f_{c\,\max}}/2)+\mathrm{BW}_{\mathrm{Tot}}}^{f_{c\,\max}+(\mathrm{BW}_{f_{c\,\max}}/2)+2\mathrm{BW}_{\mathrm{Tot}}} P(f)\cdot df\end{array}\right]_{\mathrm{dBW}} \tag{3}$$

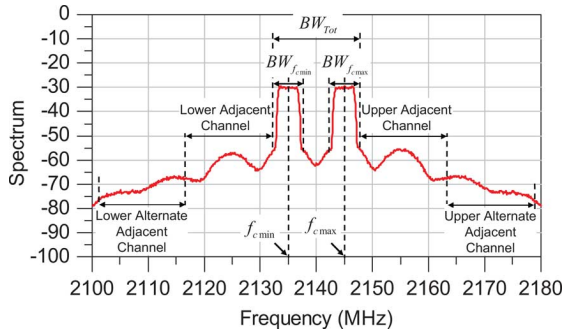

Fig. 11. MEI measurement parameters.

7) $\mathrm{BW}_{f_{c\min}}$ and $\mathrm{BW}_{f_{c\max}}$ are the bandwidth of the carriers centered around $f_{c\min}$ and $f_{c\max}$, respectively; and 8) $\mathrm{BW}_{\mathrm{Tot}}$ is the total bandwidth of the original signal spanning from and including the carriers around $f_{c\min}$ to $f_{c\max}$

$$\mathrm{BW}_{\mathrm{Tot}} = \left(f_{c\max} + \frac{\mathrm{BW}_{f_{c\max}}}{2}\right) - \left(f_{c\min} - \frac{\mathrm{BW}_{f_{c\min}}}{2}\right). \tag{4}$$

The first terms in both (2) and (3) refer to the signal power in the active carriers and is expressed in dBW. The second terms in (2) and (3) quantify the power in both the lower and upper adjacent and alternate channels, respectively. When unused carriers are available in between the active carriers, it is possible to define the MEI in the in-band by considering the power in all the unused channels situated within the total bandwidth of the original signal by

$$\mathrm{MEI}_{\mathrm{Inband}} = \left[\sum_{i=1}^{M}\int_{f_{ci}-\mathrm{BW}_i/2}^{f_{ci}+\mathrm{BW}_i/2} P(f)\cdot df\right]_{\mathrm{dBW}} - \left[\sum_{j=1}^{N}\int_{f_{cj}-\mathrm{BW}_j/2}^{f_{cj}+\mathrm{BW}_j/2} P(f)\cdot df\right]_{\mathrm{dBW}}. \tag{5}$$

This in-band MEI is calculated for the OFF channels only. It is possible to include the MEI present in the ON channels within the in-band MEI defined in (5). However, this requires the cancellation of the signal in these channels. Such a procedure is very sensitive to any gain and phase imbalance in both signals paths.

The total MEI $(\mathrm{MEI}_{\mathrm{Total}})$ can be defined as (6), shown at the bottom of this page. In the case of signals having up to four carriers, it has been found that the signal power in the active carriers can be calculated by integrating the power over the entire total bandwidth (including the unused carriers) without introducing a significant error. This is due to the fact that the $\mathrm{MEI}_{\mathrm{Inband}}$ is around 48 dBc in the case of a 1001 signal. In addition, it is worth mentioning that the $\mathrm{MEI}_{\mathrm{AdjCha}}$ and $\mathrm{MEI}_{\mathrm{AltAdjCha}}$ definitions can be adapted to standard ACPR measurements by considering separately the upper and lower adjacent channel and alternate adjacent channel, respectively, and by adjusting the power integration band, including the center frequency and the integration bandwidth. In this case, for standards compliant measurements, the nominal receiving filter of the WCDMA signal (a raised root cosine filter) needs to be applied to the post-compensated signal.

For the considered WCDMA signals, the carrier bandwidth used for power integration is 5 MHz. This guarantees consistency in the calculation, in the sense that, for adjacent channels spaced by 5 MHz, the total power will be equal to the sum of the power in the different channels. When different types of drive signals are applied (multistandards), the bandwidths used for the power integration can be adjusted separately in accordance with the type of transmitted signals in each carrier.

The adjacent channel and alternate adjacent channel MEI were calculated for the considered Doherty PA when driven by the different signals presented in Section II. For each signal drive, two post-compensators were considered: the "true" static nonlinearity and the average static nonlinearity. While the "true" static nonlinearity is independent of the drive signal, the average static nonlinearity for each drive signal corresponds to the static nonlinearity extracted by averaging the measurement data corresponding to the characterization of the PA under that test signal. Indeed, the "true" static nonlinearity refers to the static nonlinearity measured with the narrowband signal for which the DUT is memoryless (in this case, for $\alpha = 0.2$). Conversely, the averaged static nonlinearity refers to the static nonlinearity measured with the actual WCDMA test signal (single carrier or multicarrier). The results are reported in Table II. According to these results, the MEI increases as the bandwidth of the signal increases. Also, for a given bandwidth, the MEI is slightly higher when unused carriers are present within the signal bandwidth. Furthermore, the MEI obtained using the "true" static nonlinearity is close to that obtained using a post-compensator based on the averaged static nonlinearity. The error between these two cases is limited to approximately 1.5 dB for the considered signals. In addition, the averaged

$$\mathrm{MEI}_{\mathrm{Tot}} = \left[\sum_{i=1}^{M}\int_{f_{ci}-\mathrm{BW}_i/2}^{f_{ci}+\mathrm{BW}_i/2} P(f)\cdot df\right]_{\mathrm{dBW}} - \left[\begin{array}{c}\left(\begin{array}{c}\int_{f_{c\min}-(\mathrm{BW}_{f_{c\min}}/2)-\mathrm{BW}_{\mathrm{Tot}}}^{f_{c\min}-\mathrm{BW}_{f_{c\min}}/2} P(f)\cdot df \\ +\int_{f_{c\max}+\mathrm{BW}_{f_{c\max}}/2}^{f_{c\max}+(\mathrm{BW}_{f_{c\max}}/2)+\mathrm{BW}_{\mathrm{Tot}}} P(f)\cdot df\end{array}\right) \\ +\left(\begin{array}{c}\int_{f_{c\min}-(\mathrm{BW}_{f_{c\min}}/2)-2\mathrm{BW}_{\mathrm{Tot}}}^{f_{c\min}-(\mathrm{BW}_{f_{c\min}}/2)-\mathrm{BW}_{\mathrm{Tot}}} P(f)\cdot df + \\ \int_{f_{c\max}+(\mathrm{BW}_{f_{c\max}}/2)+\mathrm{BW}_{\mathrm{Tot}}}^{f_{c\max}+(\mathrm{BW}_{f_{c\max}}/2)+2\mathrm{BW}_{\mathrm{Tot}}} P(f)\cdot df\end{array}\right) \\ +\left(\sum_{j=1}^{N}\int_{f_{cj}-\mathrm{BW}_j/2}^{f_{cj}+\mathrm{BW}_j/2} P(f)\cdot df\right)\end{array}\right]_{\mathrm{dBW}} \tag{6}$$

TABLE II
MEI VERSUS DRIVE SIGNAL

Post-compensator ⇨	"True" static nonlinearity (dBc)	Averaged static nonlinearity (dBc)
Signal ⇩		
WCDMA 1C	$MEI_{AC} = 51.16$ $MEI_{AAC} = 54.23$ $MEI_{Tot} = 49.43$	$MEI_{AC} = 52.46$ $MEI_{AAC} = 54.43$ $MEI_{Tot} = 50.34$
WCDMA 2C (11)	$MEI_{AC} = 43.82$ $MEI_{AAC} = 50.89$ $MEI_{Tot} = 43.05$	$MEI_{AC} = 45.37$ $MEI_{AAC} = 51.11$ $MEI_{Tot} = 44.35$
WCDMA 3C (101)	$MEI_{AC} = 38.82$ $MEI_{AAC} = 45.51$ $MEI_{Tot} = 37.98$	$MEI_{AC} = 39.38$ $MEI_{AAC} = 45.91$ $MEI_{Tot} = 38.51$
WCDMA 3C (111)	$MEI_{AC} = 40.19$ $MEI_{AAC} = 47.30$ $MEI_{Tot} = 39.42$	$MEI_{AC} = 41.11$ $MEI_{AAC} = 47.82$ $MEI_{Tot} = 40.27$
WCDMA 4C (1001)	$MEI_{AC} = 36.13$ $MEI_{AAC} = 36.91$ $MEI_{Tot} = 33.49$	$MEI_{AC} = 36.20$ $MEI_{AAC} = 38.11$ $MEI_{Tot} = 34.04$
WCDMA 4C (1111)	$MEI_{AC} = 37.58$ $MEI_{AAC} = 40.50$ $MEI_{Tot} = 35.79$	$MEI_{AC} = 38.23$ $MEI_{AAC} = 41.06$ $MEI_{Tot} = 36.41$

static nonlinearity always gives a lower residual nonlinearity at the output of the static post-compensator. Accordingly, it is expected that a memoryless DPD derived using the averaged static nonlinearity will lead to a slightly better linearization, compared to the case where a memoryless DPD derived using the "true" static nonlinearity is applied.

VI. CONCLUSION

In this paper, an accurate experimental approach for static nonlinearity extraction suitable for RF PAs/transmitters exhibiting memory effects was presented. In this technique, the input waveform is resampled at a lower sampling rate to reduce its bandwidth and, thus, decrease the memory effects exhibited by the DUT. It was shown that memory effects influence the averaged static nonlinearity. In addition, a characterization of the static nonlinearity over the entire 2100-MHz cellular band brings to light the frequency dependency of the static nonlinearity. The measured static nonlinearity variation versus frequency showed the dependency of the nonlinearity shape on the carrier frequency that adds up to the conventional frequency response of the PA (small-signal gain variation versus frequency). This contributes to the nonlinear behavior exhibited by the PA when driven by wideband modulated signals.

The static nonlinearity characteristic was then used to develop a memoryless post-compensation technique that was proposed for model accuracy assessment. This technique minimizes the number of measurements required for model validation when compared to existing static nonlinearity pre-compensation techniques. In addition, it was demonstrated, through the use of six state-of-the-art behavioral models, that the memoryless post-compensation technique is needed to accurately assess the performance of the models and their ability to predict the memory effects exhibited by the DUT.

Finally, memoryless post-compensation was used to evaluate the MEI of the Doherty PA, when driven by several multicarrier WCDMA signals. This metric is crucial for objective head-to-head comparison of the behavior of PAs/transmitters prototypes.

The combination of the extraction and use of "true" static nonlinearity along with the post-compensation technique allows accurate and quick assessment of memory effects impact and intensity in wideband highly nonlinear RF PAs and transmitters driven by modulated signals. In addition, the proposed MEI metrics can be used to quantify this impact. This offers a comprehensive approach and a valuable tool for research and development engineers to quickly and accurately characterize and compare PAs/transmitters and study their linearizability.

REFERENCES

[1] A. Zhu, J. C. Pedro, and J. T. Brazil, "Dynamic deviation reduction-based Volterra behavioral modeling of RF power amplifiers," *IEEE Trans. Microw. Theory Tech.*, vol. 54, no. 12, pp. 4323–4332, Dec. 2006.

[2] O. Hammi, F. M. Ghannouchi, and B. Vassilakis, "A compact envelope-memory polynomial for RF transmitters modeling with application to baseband and RF-digital predistortion," *IEEE Microw. Wireless Compon. Lett.*, vol. 18, no. 5, pp. 359–361, May 2008.

[3] O. Hammi, F. M. Ghannouchi, S. Boumaiza, and B. Vassilakis, "A data-based nested LUT model for RF power amplifiers exhibiting memory effects," *IEEE Microw. Wireless Compon. Lett.*, vol. 17, no. 10, pp. 712–714, Oct. 2007.

[4] H. C. Ku, M. D. McKinley, and J. S. Kenney, "Quantifying memory effects in RF power amplifiers," *IEEE Trans. Microw. Theory Tech.*, vol. 50, no. 12, pp. 2843–2849, Dec. 2002.

[5] M. Isaksson, D. Wisell, and D. Ronnow, "A comparative analysis of behavioral models for RF power amplifiers," *IEEE Trans. Microw. Theory Tech.*, vol. 54, no. 1, pp. 348–359, Jan. 2006.

[6] B. Vassilakis and A. Cova, "A comparative analysis of GaAs/LDMOS/GaN high power transistors in a digital predistortion amplifier system," in *Proc. IEEE Asia–Pacific Microw. Conf.*, Dec. 2005, vol. 2, 4 pp.

[7] T. Liu, Y. Ye, S. Boumaiza, X. Zeng, J. He, A. B. Sesay, and F. M. Ghannouchi, "Accurate validation methods for dynamic nonlinear behavior models of wideband RF power amplifiers using memoryless predistortion techniques," in *IEEE Int. Microw., Antennas, Propag., and EMC Technol. Wireless Commun. Symp.*, Hangzhou, China, Aug. 2007, pp. 358–361.

[8] T. Liu, S. Boumaiza, A. B. Sesay, and F. M. Ghannouchi, "Quantitative measurements of memory effects in wideband RF power amplifiers driven by modulated signals," *IEEE Microw. Wireless Compon. Lett.*, vol. 17, no. 1, pp. 79–81, Jan. 2007.

[9] T. Liu, S. Boumaiza, and F. M. Ghannouchi, "Deembedding static nonlinearities and accurately identifying and modeling memory effects in wideband RF transmitters," *IEEE Trans. Microw. Theory Tech.*, vol. 53, no. 11, pp. 3578–3587, Nov. 2005.

[10] M. E. Gardinger, D. Silveira, and G. Magerl, "Efficient power amplifier identification using modified parallel cascade Hammerstein models," in *IEEE Radio Wireless Symp. Dig.*, Jan. 2007, pp. 305–308.

[11] J. P. Martins, P. M. Cabral, N. B. Carvalho, and J. C. Pedro, "A metric for the quantification of memory effects in power amplifiers," *IEEE Trans. Microw. Theory Tech.*, vol. 54, no. 12, pp. 4432–4439, Dec. 2006.

[12] J. Vuolevi, T. Rahkonen, and J. P. A. Manninen, "Measurement technique for characterizing memory effects in RF power amplifiers," *IEEE Trans. Microw. Theory Tech.*, vol. 49, no. 8, pp. 1383–1389, Aug. 2001.

[13] H. C. Ku, M. D. McKinley, and J. S. Kenney, "Quantifying memory effects in RF power amplifiers," *IEEE Trans. Microw. Theory Tech.*, vol. 50, no. 12, pp. 2843–2849, Dec. 2002.
[14] D. Ronnow, D. Wisell, and M. Isaksson, "Three-tone characterization of nonlinear memory effects in radio-frequency power amplifiers," *IEEE Trans. Instrum. Meas.*, vol. 56, no. 6, pp. 2646–2657, Dec. 2007.
[15] P. Draxler, J. Deng, D. Kimball, I. Langmore, and P. M. Asbeck, "Memory effect evaluation and predistortion of power amplifiers," in *IEEE MTT-S Int. Microw. Symp. Dig.*, Jun. 2005, pp. 1549–1552.
[16] J. Dunsmore and D. Goldberg, "Novel two-tone intermodulation phase measurement for evaluating amplifier memory effects," in *Proc. IEEE Eur. Microw. Conf.*, Oct. 2003, pp. 235–238.
[17] O. Hammi, S. Carichner, B. Vassilakis, and F. M. Ghannouchi, "Novel approach for static nonlinear behavior identification in RF power amplifiers exhibiting memory effects," in *IEEE MTT-S Int. Microw. Symp. Dig.*, Jun. 2008, pp. 1521–1524.
[18] E. G. Jeckeln, F. Beauregard, M. A. Sawan, and F. M. Ghannouchi, "Adaptive baseband/RF predistorter for power amplifiers through instantaneous AM–AM and AM–PM characterization using digital receivers," in *IEEE MTT-S Int. Microw. Dig.*, Jun. 2000, pp. 489–492.

Oualid Hammi (S'03) received the B.Eng. degree in electrical engineering from the École Nationale d'Ingénieurs de Tunis, Tunis, Tunisia, in 2001, the M.Sc. degree from the École Polytechnique de Montréal, Montréal, QC, Canada, in 2004, and is currently working toward the Ph.D. degree at the Schulich School of Engineering, University of Calgary, Calgary, AB, Canada.

He is currently with the iRadio Laboratory, Schulich School of Engineering, University of Calgary. His current research interests are in the area of digital signal processing, and in general, microwave and millimeter-wave engineering. His particular research activities are related to the design of highly efficient linear transmitters for wireless communication systems and the characterization, behavioral modeling, and linearization of highly nonlinear RF PAs.

Scott Carichner (S'85–M'02) received the B.S. degree in electrical engineering at the University of Illinois at Urbana-Champaign, in 1987, and the M.S. degree in electrical engineering from Stanford University, Stanford, CA, in 1989.

He was with Sandia National Laboratories, Livermore, CA, for 12 years, during which time he performed research into complex systems while jointly conducting postgraduate studies at Stanford University. In 2002, he joined Powerwave Technologies Inc., where he is currently a Senior Principal Engineer with the Research and Systems Group, conducting research on high-efficiency amplifiers, digital predistortion techniques, and various analog and digital signal processing techniques for wireless communication systems.

Bill Vassilakis (M'88–SM'05) received the B.Eng. degree in electrical engineering from McGill University, Montreal, QC, Canada, in 1985.

He is currently Senior Vice President, Global Research and Product Development with Powerwave Technologies Inc., Santa Ana, CA. His responsibilities include leading a global team developing advanced components and solutions for wireless communication networks. During the past 12 years under his direction, the Intellectual Property portfolio of Powerwave Technologies Inc. has grown to include over 430 worldwide patents in amplifier, antenna, filter, and digital signal processing technology. He has previously held positions with Northern Telecom (1985–1990), where he was involved with microwave radio design, prior to working for NovAtel, Calgary, AB, Canada (1990–1992), where he designed components for digital cellular systems. From 1992 to 1996, he was with MA/COM, Burlington, MA, as Lead Designer in their commercial PA organization. He has authored or coauthored over 30 technical papers. He holds six U.S. patents.

Mr. Vassilakis is a Registered Professional Engineer.

Fadhel M. Ghannouchi (S'84–M'88–SM'93–F'07) is currently a Professor and iCORE/CRC Chair with the Electrical and Computer Engineering Department, The Schulich School of Engineering, University of Calgary, Calgary, AB, Canada, and Director of the Intelligent RF Radio Laboratory. He has held several invited positions with several academic and research institutions in Europe, North America, and Japan. He has provided consulting services to a number of microwave and wireless communications companies. He has authored or coauthored over 400 publications. He holds ten U.S. patents with three pending. His research interests are in the areas of microwave instrumentation and measurements, nonlinear modeling of microwave devices and communications systems, design of power and spectrum efficient microwave amplification systems, and design of intelligent RF transceivers for wireless and satellite communications.